



Crystallization and microstructure of Eu^{3+} -doped lithium aluminophosphate glass



Roque S. Soares^a, Regina C.C. Monteiro^{a,*}, Andreia A.S. Lopes^a, Maria M.R.A. Lima^a, Bogdan A. Sava^b, Mihail Elisa^b

^a Department of Materials Science, CENIMAT/IBN, Faculty of Sciences and Technology, Universidade Nova de Lisboa, 2825-516 Caparica, Portugal

^b Department of Optoelectronics, National Institute of R & D for Optoelectronics, INOE 2000, 77125 Magurele, Romania

ARTICLE INFO

Article history:

Received 30 May 2014

Received in revised form 27 June 2014

Available online xxxx

Keywords:

Aluminophosphate glasses;

Differential thermal analysis;

Crystallization kinetics;

Activation energy;

Microstructure

ABSTRACT

A transparent Eu^{3+} -doped lithium aluminophosphate glass was prepared by melt-quenching technique. The thermal behavior of the glass was investigated by differential thermal analysis (DTA), the structure was studied by X-ray diffraction (XRD) and the morphology was observed by optical polarization microscopy and scanning electron microscopy (SEM). The activation energy of glass transition and the activation energy of crystallization and Avrami exponent have been evaluated under non-isothermal conditions from the data obtained by DTA at different heating rates. DTA curves exhibited an endothermic peak associated with the glass transition and two exothermic peaks. The mean value calculated for the activation energy of glass transition was 545 kJ mol^{-1} . The activation energy of crystallization was $\sim 400 \text{ kJ mol}^{-1}$ for the first exothermic peak and $\sim 170 \text{ kJ mol}^{-1}$ for the second peak. The Avrami exponent was ~ 1 for both peaks indicating surface crystallization. XRD results showed that the main crystalline phase, aluminum metaphosphate, $\text{Al}(\text{PO}_3)_3$, and aluminum phosphate, AlPO_4 , were formed together with lithium barium phosphate, $\text{Li}_3\text{Ba}(\text{PO}_3)_7$, during the first exothermic peak and together with barium pyrophosphate, $\text{Ba}_2\text{P}_2\text{O}_7$, during the second peak. Morphological study of heat-treated glass samples revealed microstructural features that confirmed a surface crystallization process.

© 2014 Elsevier B.V. All rights reserved.

1. Introduction

Rare-earth (RE) doped phosphate glasses have attracted considerable interest in recent years because of their technological interest particularly for optical applications. Phosphate glasses are excellent host materials for RE ions due to advantageous local structure effect and high RE ion solubility [1]. The photosensitivity of RE doped phosphate glasses makes these materials attractive for lasers, amplifiers, photosensitivity sensors, optical storage and Faraday rotators [2–6].

High thermal stability and transparency of the lithium aluminophosphate glasses are fundamental properties for the applications of this host in photonics and optoelectronics. The understanding of the crystallization behavior is a prerequisite for most of the applications, as stability against crystallization determines their effective working limits [7,8]. In the previous studies, some of the authors reported the optical properties and structural characteristics of a Eu^{3+} doped lithium aluminophosphate glass with a molar composition $20.4\text{Li}_2\text{O}-7.2\text{BaO}-10.3\text{Al}_2\text{O}_3-1.4\text{La}_2\text{O}_3-58.5\text{P}_2\text{O}_5-2.1\text{Eu}_2\text{O}_3$ [2,4]. The objectives of the present work are to investigate the crystallization behavior of this glass, to identify the phases formed after crystallization and to analyze

the microstructural evolution. The influence of glass crystallization on the luminescence of Eu^{3+} ions will be addressed in the future work.

Differential thermal analysis (DTA) and differential scanning calorimetry (DSC) are widely used to investigate the crystallization kinetics of a glass. To determine the crystallization parameters such as the activation energy of crystallization (E_c) and the Avrami exponent (n) in Johnson–Mehl–Avrami (JMA) equation [9–12], for the present glass, non-isothermal methods were employed. The variations of activation energy and of Avrami exponent with the fraction of crystallization were evaluated. XRD was used to identify the crystalline phases that precipitated in the heat-treated glass samples. Optical microscopy and SEM were used to analyze the evolution of microstructural features during the non-isothermal treatment, the results being discussed together with the values calculated for the Avrami exponent to analyze the mechanisms of crystallization.

2. Material preparation and experimental procedure

The Eu^{3+} doped lithium aluminophosphate glass, with a nominal composition $20.4\text{Li}_2\text{O}-7.2\text{BaO}-10.3\text{Al}_2\text{O}_3-1.4\text{La}_2\text{O}_3-58.5\text{P}_2\text{O}_5-2.1\text{Eu}_2\text{O}_3$ (mol.%), was prepared by melt quenching technique using analar grade chemicals, Li_2CO_3 , BaCO_3 , Al_2O_3 , La_2O_3 , H_3PO_4 and Eu_2O_3 . The preparation procedure was similar to that used for RE-doped aluminophosphate glasses reported in the previous work [13]. The

* Corresponding author. Tel.: +351 212948564; fax: +351 212957810.
E-mail address: rcm@fct.unl.pt (R.C.C. Monteiro).

reagents were introduced in H_3PO_4 solution, mixed by continuous stirring, and then the mixture was heated and dried until the batch viscosity was significantly increased. This homogenization and drying step is accompanied by the releasing of gasses resulting from chemical reactions, which take place at ~ 473 K. In this way, homogeneous metaphosphates are formed, improving the chemical homogeneity of the final glass [13]. The dried mixture, with ~ 130 g, was heated in an alumina crucible in two steps: at a heating rate of 100 K h^{-1} from room temperature up to 973 K, to eliminate volatile components (CO_2), and then at a heating rate of 250 K h^{-1} up to 1523 K, with a 4 h holding at this temperature to achieve glass melting and refining. To improve the glass chemical homogeneity and to obtain a vitreous material with a minimum of defects (e.g., gas bubbles and cords), stirring of the melt was carried out, using a corundum stirrer, at a rotation speed between 100 and 250 rot min^{-1} , depending on the temperature and viscosity of the glass melt. After melting, the glass was cast in graphite molds and annealed at 723 K for 6 h to avoid internal strains.

DTA tests were performed in a thermal analyzer equipment (STA PT 1600, Linseis, Germany), using 50 mg glass powder samples (with a particle size smaller than $65\text{ }\mu\text{m}$) that were heated inside an alumina crucible, in static air, from room temperature up to a maximum temperature of 1173 K, at various heating rates ($5, 10, 15$ and 25 K min^{-1}) and using an empty crucible as reference. From the DTA curves, the glass transition temperature (T_g), the onset crystallization temperature (T_c) and the peak crystallization temperature (T_p) were determined using the software associated with the equipment, and the measurement error is assumed as 1%. Glass samples with sizes of $\sim 7\text{ mm} \times 7\text{ mm} \times 2\text{ mm}$ were heated in an electric tubular furnace at 5 K min^{-1} to a selected temperature, suggested by the DTA results, and held at that temperature for 2 h. The amorphous nature of the as-prepared glass and the crystalline phases formed in heat-treated glass were identified by XRD analysis of finely ground samples, performed on a diffractometer (Dmax III-C 3 kW, Rigaku Corporation, Tokyo, Japan), using $CuK\alpha$ radiation at 40 kV and 30 mA settings in the 2θ range from 20° to 60° , an acquisition time of 1 s and 2θ increment of 0.04° . Crystalline phases were identified by comparing the peak positions and intensities with those listed in the software standard files (ICDD, Newtown Square, PA, USA). The microstructure of heat-treated glass samples was observed using a polarization optical microscope (Olympus-BX51 TRF, USA) and a scanning electron microscope (SEM-FIB – Zeiss Auriga, Germany). To reduce the charge effects, as the samples are nonconductive, they were fixed to the holder with a carbon tape and coated with $\sim 4\text{ nm Au/Pd}$ before SEM observation. For elemental chemical analysis, energy dispersive spectroscopy (EDS, Oxford INCA, Energy 350) was employed.

3. Results

3.1. Differential thermal analysis

Fig. 1 shows DTA curves for the glass obtained at different heating rates (in the range $5\text{--}25\text{ K min}^{-1}$). The values of the glass transition temperature (T_g), of the onset crystallization temperatures (T_{c1} and T_{c2}) and of the maxima of the exothermic peaks (T_{p1} and T_{p2}) for the different heating rates are summarized in Table 1.

3.2. Glass transition analysis

Three approaches were used to analyze the dependence of glass transition temperature (T_g) on the heating rate (β). The first was the empirical relationship according to Lasocka that can be written in the following form [14]:

$$T_g = A_g + B_g \log \beta \quad (1)$$

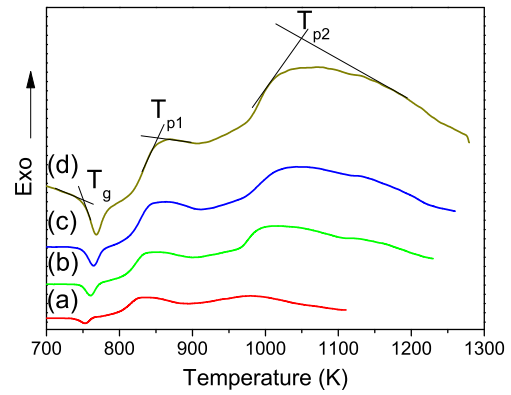


Fig. 1. DTA curves for the glass at 5 K min^{-1} (a), 10 K min^{-1} (b), 15 K min^{-1} (c) and 25 K min^{-1} (d).

where A_g and B_g are constants for a given glass composition [14]. According to Eq. (1), the constant A_g corresponds to T_g at $\beta = 1\text{ K min}^{-1}$, and B_g reflects the dependence of the structural changes within the glass transition region of the supercooled liquid on the heating rate [14]. The value of B_g is related to the method of quenching the glass, the lower the cooling rate of the melt, the lower the B_g value [14].

Fig. 2 shows the plot of T_g versus $\log \beta$, a straight regression line fitted to the experimental data and Eq. (1) written for the particular case of this glass. The inset in the figure shows clearly an upward shift in T_g with the increase in β .

The second approach used to analyze the dependence of T_g on β was based on Kissinger's method [15], which can be used to estimate the activation energy associated with the glass transition (E_g) under non-isothermal treatment schedules, according to the following equation:

$$\ln \left(\frac{\beta}{T_g^2} \right) = - \frac{E_g}{RT_g} + \text{const.} \quad (2)$$

where R is the universal gas constant. Although Kissinger equation is mainly used for the determination of the activation energy of crystallization, it has also been used to calculate E_g [16]. A plot of $\ln(\beta/T_g^2)$ versus $(1000/T_g)$ gives a linear relation, which is illustrated in Fig. 3. From the slope of the straight regression line fitted to the experimental data, the value of E_g was calculated ($537 \pm 16\text{ kJ mol}^{-1}$). Assuming that the variation of $\ln(1/T_g^2)$ with β is much slower than that of $\ln(1/T_g)$ with $\ln \beta$ [17], another approach has been used to calculate E_g :

$$\ln \beta = - \frac{E_g}{RT_g} + \text{const.} \quad (3)$$

A plot of $\ln \beta$ against $1000/T_g$ and a straight line fitted to the experimental data are also shown in Fig. 3. From the slope of the straight line the value of E_g was obtained ($550 \pm 16\text{ kJ mol}^{-1}$).

Table 1

Glass transition temperature (T_g), and onset (T_{c1} and T_{c2}) and peak (T_{p1} and T_{p2}) crystallization temperatures determined from DTA data at different heating rates.

Heating rate, β (K/min)	T_g (K)	Peak1		Peak2	
		T_{c1} (K)	T_{p1} (K)	T_{c2} (K)	T_{p2} (K)
5	740	774	830	897	980
10	747	794	838	945	1008
15	750	798	845	958	1027
25	753	810	853	968	1057

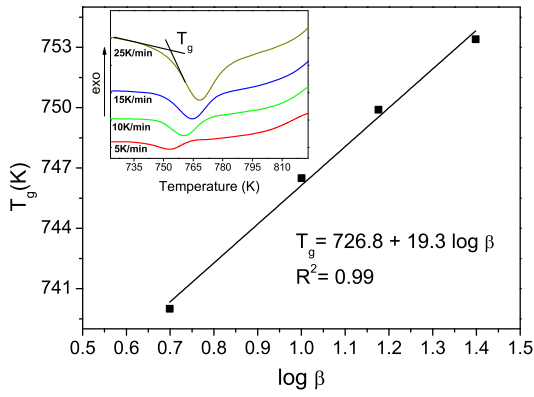


Fig. 2. Plot of T_g versus $\log \beta$. The inset shows the glass transition peaks observed at four different heating rates.

3.3. Crystallization kinetics

Kissinger [15] method is widely used for analyzing crystallization during DSC or DTA experiments. According to this method, the activation energy for crystallization (E_c) is evaluated through the variation of T_p with β given by the following equation:

$$\ln\left(\frac{\beta}{T_p^2}\right) = -\frac{E_c}{RT_p} + const. \quad (4)$$

By plotting $\ln(\beta/T_p^2)$ against $1000/T_p$ for the first and second exothermic peaks, the values of the activation energy (E_{c1} and E_{c2}) were calculated from the slopes of the straight regression lines fitted to the experimental data as shown in Fig. 4(a–b), and are listed in Table 2. Alternatively, the activation energy for crystallization was calculated according to the method suggested by Ozawa [18], using the following equation [16,18]:

$$\ln \beta = -\frac{E_c}{RT_p} + const. \quad (5)$$

From the linear plot of $\ln \beta$ versus $1/T_p$, also shown in Fig. 4, the values of E_{c1} and E_{c2} , were obtained from the slopes, and are also presented in Table 2.

The fraction of crystallization (χ) at any temperature (T) has been determined from the DTA curves at each heating rate by the ratio $\chi = A_T/A$ [16]. A is the total area of the exothermic peak between the temperature T_i (where crystallization just begins) and the temperature T_f (where the crystallization is completed) and A_T is the partial area

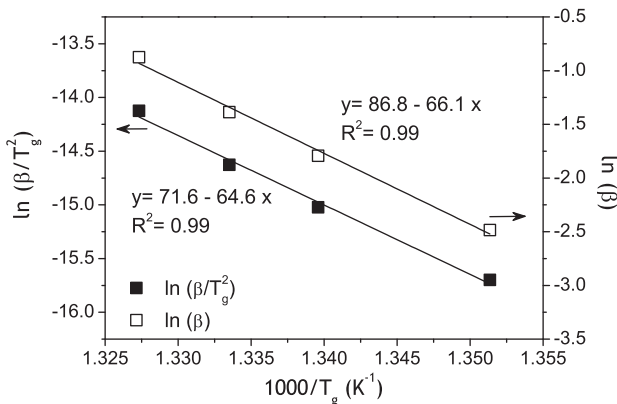


Fig. 3. Plots of $\ln(\beta/T_g^2)$ and of $\ln(\beta)$ versus $1000/T_g$.

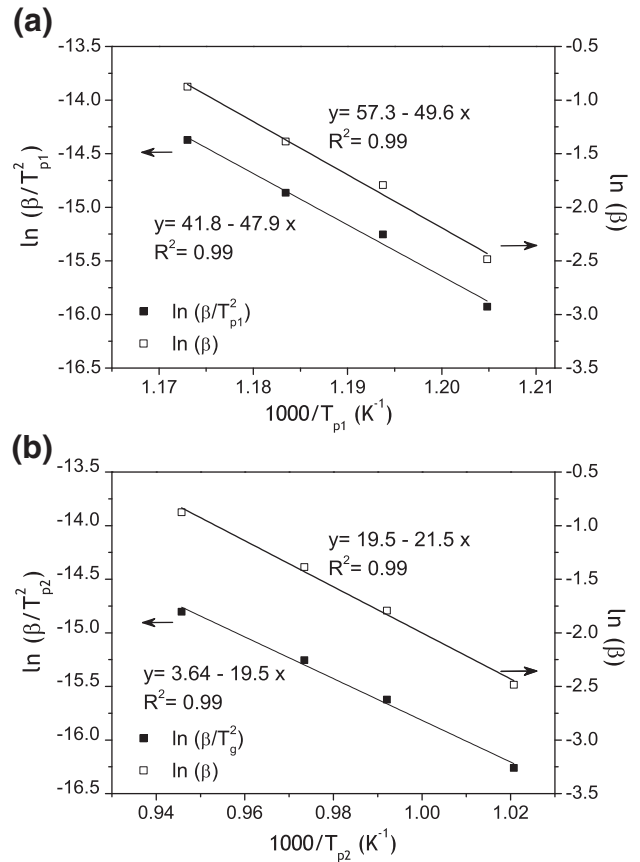


Fig. 4. Plots of $\ln(\beta/T_p^2)$ and of $\ln \beta$ versus $1000/T_p$ for the first exothermic peak (a) and second exothermic peak (b).

between T_i and T , as illustrated schematically in Fig. 5. The plot of χ as a function of temperature for both exothermic peaks is shown in Fig. 6.

The ratio between the ordinate of the DTA curve and the total area of the peak gives the corresponding crystallization rate ($d\chi/dt$) [19]. From the plot of $d\chi/dt$ as a function of temperature for both exothermic peaks, shown in Fig. 7(a–b), the maximum $(d\chi/dt)_{T_p}$ was determined for every heating rate. According to the method proposed by Gao and Wang [20], from the experimental values of the maximum crystallization rate, $(d\chi/dt)_{T_p}$, it is possible to calculate the Avrami exponent (n) using the following equation [20–22]:

$$n = \left(\frac{d\chi}{dt}\right)_{T_p} \frac{RT_p^2}{0.37\beta E_c}. \quad (6)$$

Using Eq. (6), the kinetic exponent n at each experimental heating rate was determined for both peaks, considering the values obtained for the activation energy of crystallization for the two peaks (E_{c1} and E_{c2}). The mean values of Avrami exponent obtained for the first and second peaks are listed in Table 2.

Table 2
Estimated values of activation energy of crystallization (E_c) and of Avrami exponent (n) for the first and second exothermic peaks.

Method	Peak1		Peak2	
	E_{c1} (kJ mol ⁻¹)	$\langle n \rangle$	E_{c2} (kJ mol ⁻¹)	$\langle n \rangle$
Kissinger	398 ± 14		162 ± 14	
Ozawa	412 ± 14		179 ± 14	
Gao–Wang		0.91 ± 0.02		0.97 ± 0.24

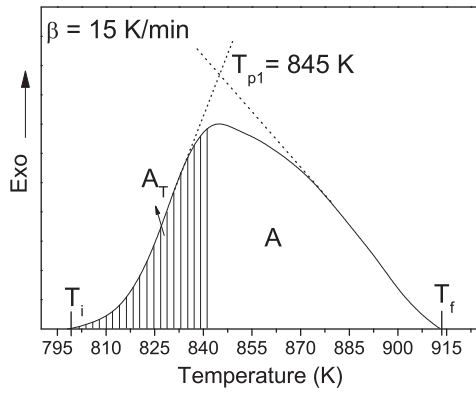


Fig. 5. Illustration of area A between T_i and T_f , and of area A_T between T_i and T (T_i , T_f and T according to text) for the first exothermic peak in a DTA curve at a heating rate of 15 K/min.

According to the modified Ozawa equation, proposed by Matusita et al. [23], in a non-isothermal crystallization process, the fraction crystallized (χ) in an as-quenched glass heated at constant rate (β) is related to the activation energy of crystallization (E_c) through the following expression [23]:

$$\ln[-\ln(1-\chi)] = -n \ln\beta - 1.052(n-1)(E_c/RT) + \text{const.} \quad (7)$$

For each heating rate, the plot of $\ln[-\ln(1-\chi)]$ versus $1000/T$ should be a straight line. However, non-linear plots were obtained, as shown in Fig. 8(a–b), suggesting that there is a variation of E_c and of n during the crystallization process of glass.

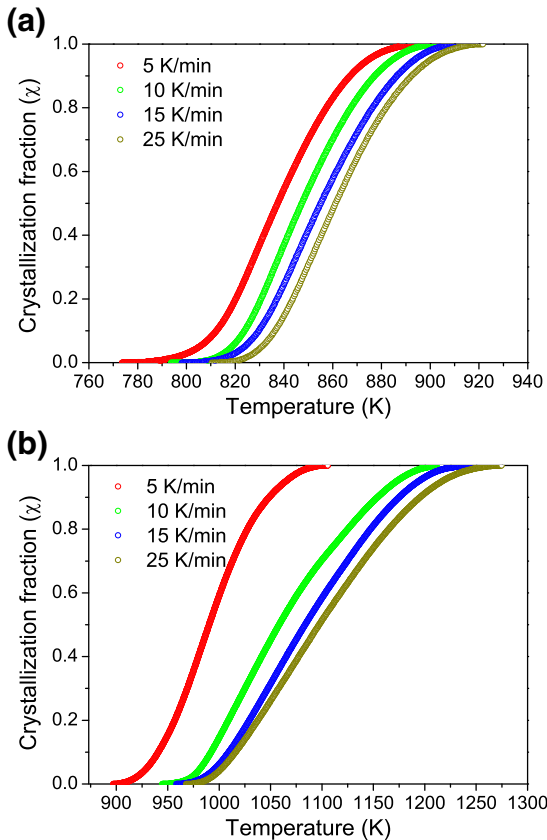


Fig. 6. Crystallization fraction (χ) as a function of temperature at different heating rates for the (a) first crystallization peak and (b) second crystallization peak.

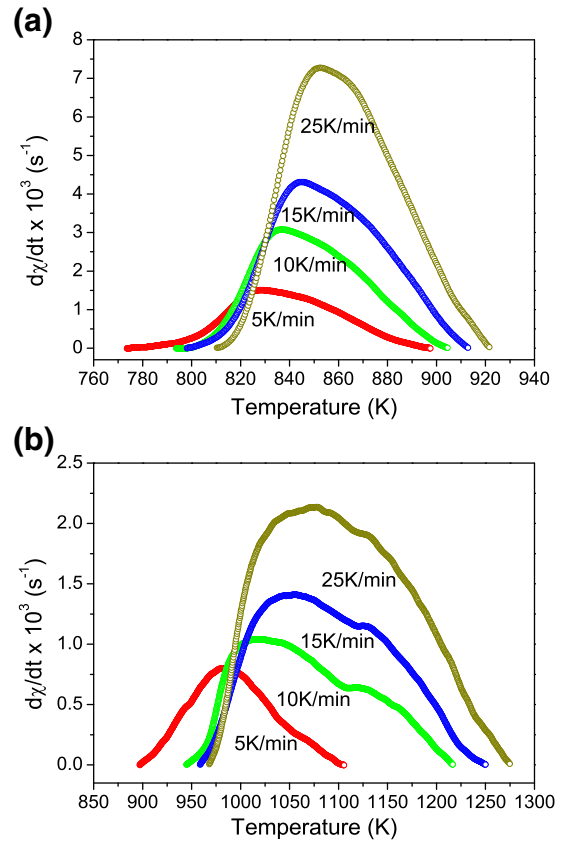


Fig. 7. Crystallization rate as a function of temperature at different heating rates for the first exothermic peak (a) and second exothermic peak (b).

An isoconversional method was employed to evaluate the activation energy of crystallization as a function of the fraction of crystallization, $E_c(\chi)$, which reflects the change of nucleation and growth behavior during the crystallization process [24,25]. The calculation of the effective activation energy, $E_c(\chi)$, was based on the method proposed by Kissinger [15], according to the following expression:

$$\left[\frac{d \ln(\beta/T^2)}{d(1/T)} \right]_{\chi} = -\frac{E_c(\chi)}{R} \quad (8)$$

where R is the gas constant, and T and β are the temperature and the heating rate corresponding to the value of χ , respectively.

Using the experimental data shown in Fig. 6(a), plots of $\ln(\beta/T^2)$ versus $1000/T$ were obtained at various values of χ for the first exothermic peak, as illustrated in Fig. 9(a). The values of $E_{c1}(\chi)$ were calculated from the slope of the straight regression lines fitted to the experimental data at the various χ . Similarly, $E_c(\chi)$ can be estimated on the basis of the method proposed by Ozawa [26], using the following equation:

$$\left[\frac{d \ln(\beta)}{d(1/T)} \right]_{\chi} = -\frac{E_c(\chi)}{R}. \quad (9)$$

Plots of $\ln \beta$ versus $1000/T$ were obtained at various values of χ for the first exothermic peak, as shown in Fig. 9(b), and $E_{c1}(\chi)$ values were calculated from the slope of the lines fitted to the experimental data at the various χ . Using the experimental data shown in Fig. 6(b), a similar procedure was adopted to calculate $E_{c2}(\chi)$ from the plots of $\ln(\beta/T^2)$ versus $1000/T$ and of $\ln \beta$ versus $1000/T$ (not shown). Fig. 10 presents the variation of $E_c(\chi)$ with the crystallized volume fraction (χ) for the two peaks. Error bars associated with $E_c(\chi)$ correspond to

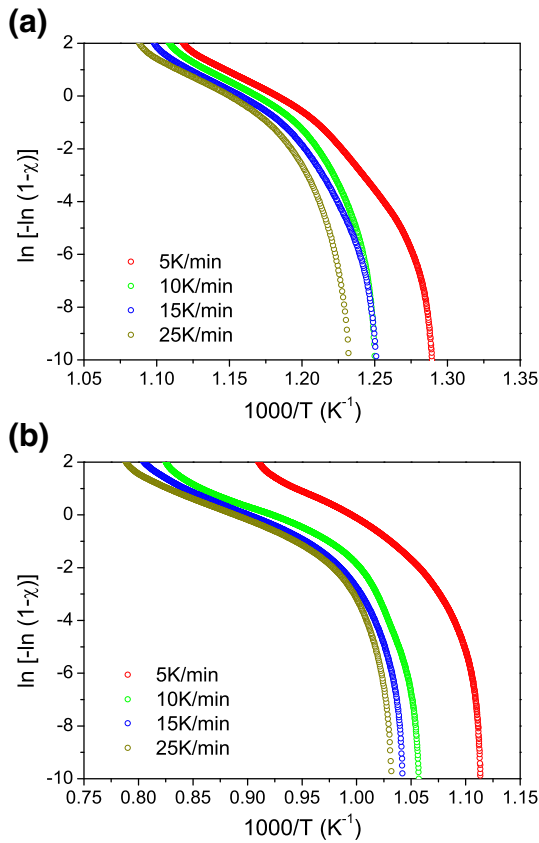


Fig. 8. Plot of $\ln[-\ln(1-\chi)]$ versus $1000/T$ at different heating rates for the first exothermic peak (a) and second exothermic peak (b).

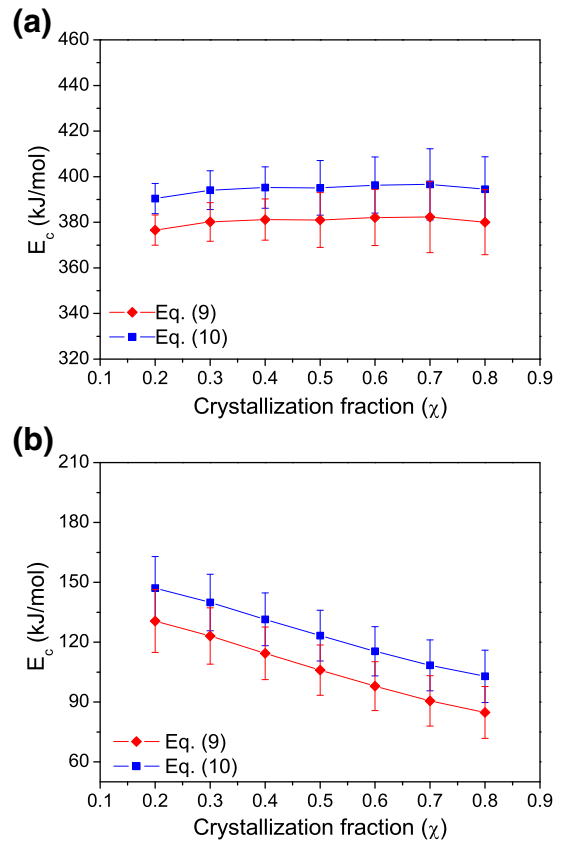


Fig. 10. Plots of $E_c(\chi)$ versus χ for the first peak (a) and second peak (b). Lines serve as guides to the eye.

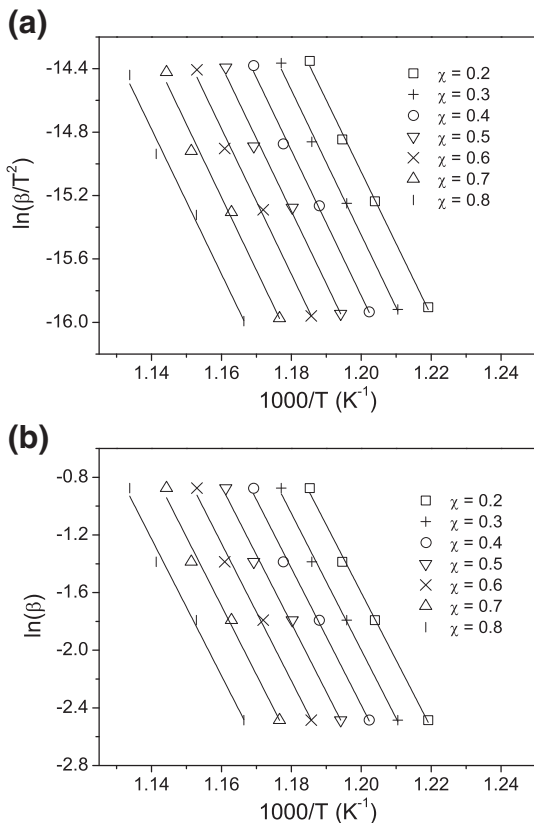


Fig. 9. Plots of $\ln(\beta/T_p^2)$ (a) and of $\ln(\beta)$ versus $1000/T_p$ for $E_c(\chi)$ determination by Kissinger and Ozawa methods, respectively.

the range of $E_c(\chi)$ values obtained for each value of crystallization fraction.

From the prior knowledge of the effective activation energy for a non-isothermal crystallization process, an equation has been proposed by Lu et al. [24] in order to calculate the Avrami exponent, which is expressed as [24]:

$$n(\chi) = \frac{-R}{E_c(\chi)} \frac{\partial \ln[-\ln(1-\chi)]}{\partial \ln(1/T)} \quad (11)$$

Taking into account the effective activation energy, $E_c(\chi)$, the Avrami exponent, $n(\chi)$, at various heating rates (5, 10, 15, 25 K min⁻¹) has been calculated using Eq. (11). Fig. 11 shows the variation of the Avrami exponent calculated at the various heating rates with the fraction of crystallization, χ , for the two exothermic peaks. Error bars associated with $n(\chi)$ correspond to the range of $n(\chi)$ values obtained for the different heating rates at a given crystallization fraction.

3.4. Characterization of heat-treated glasses by XRD

Fig. 12 presents the XRD results for glass samples heat-treated for 2 h at different temperatures. The XRD pattern of the as-prepared glass is also shown, Fig. 12(a), and it exhibits a broad hump, indicating the amorphous nature of the sample. No crystallinity was detected in the glass after heat treatment at 773 K, Fig. 12(b). For a sample treated at 823 K, Fig. 12(c), a temperature within the first DTA crystallization peak, the crystalline phases aluminum metaphosphate, $\text{Al}(\text{PO}_3)_3$, and aluminum phosphate, AlPO_4 , were identified, together with lithium barium phosphate, $\text{Li}_3\text{Ba}_2(\text{PO}_3)_7$. For a sample treated at 923 K, Fig. 12(c), a temperature within the second DTA exotherm, $\text{Al}(\text{PO}_3)_3$ and AlPO_4 were present together with barium pyrophosphate, $\text{Ba}_2\text{P}_2\text{O}_7$.

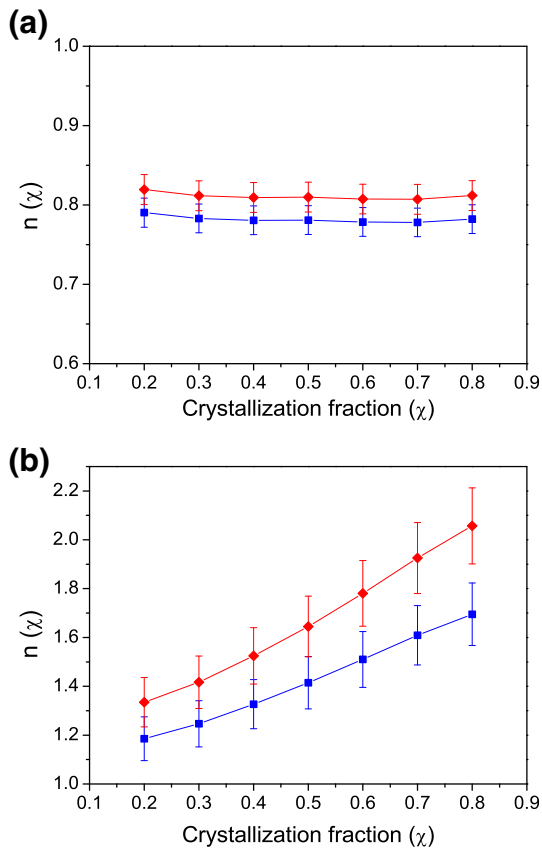


Fig. 11. Change of Avrami exponent, $n(\chi)$, as a function of crystallized fraction at the various heating rates for the first exothermic peak (a) and second exothermic peak (b). Lines serve as guides to the eye.

Crystallization at temperatures higher than 923 K was not studied due to the softening and deformation of the glass samples.

3.5. Microstructural characterization

Observation by optical microscopy (transmitted light) of the transparent as-prepared glass and of glass samples treated for 2 h at 773 K

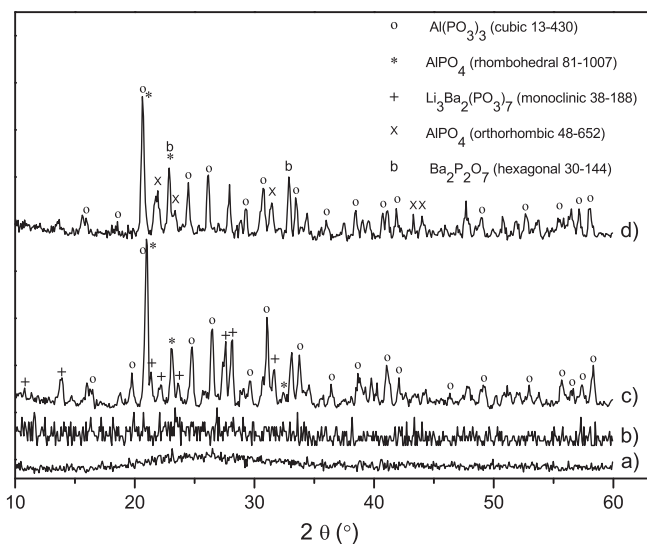


Fig. 12. XRD patterns of as-prepared glass (a) and of samples after heat-treatment for 2 h at 773 K (b), 823 K (c) and 923 K (d).

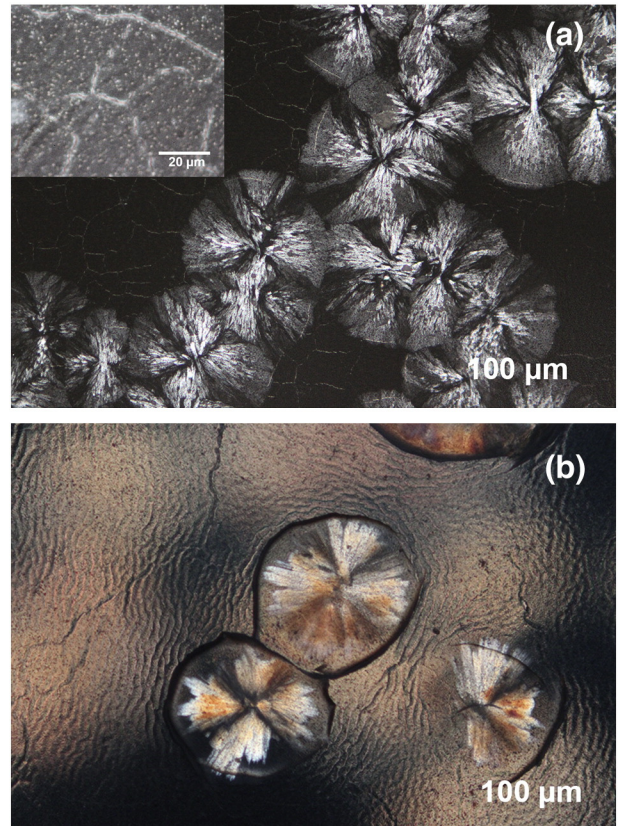


Fig. 13. Optical microscope images of glass samples heated for 2 h at 823 K (a) and 923 K (b) (crossed polarized light).

revealed their isotropic nature, appearing dark under crossed polarized light. In glass samples treated for 2 h at 823 K, “flower-like” aggregates of crystals were observed, Fig. 13(a), appearing in a non-homogeneous glass matrix showing some microstructural features, as depicted at higher magnification in the inset of Fig. 13(a). The optical microscopy image under cross-polarized light of a glass sample treated at 923 K, Fig. 13(b), shows clearly the anisotropic nature of the crystals forming “flower-like” aggregates within the glass matrix.

SEM micrographs of the crystallized glass samples are shown in Fig. 14(a–c). It is observed that the glass matrix in the sample heated at 823 K contained round-shape precipitates, Fig. 14(a), and that in the sample heated at 923 K most of the precipitates exhibited an irregular shape, Fig. 14(b). Observation at a higher magnification of the matrix of sample heated at 923 K, region M in Fig. 14(b), revealed the presence of precipitated nanocrystallites, as shown in Fig. 14(c). EDS analysis of the precipitated crystals (region C) and of the matrix (region M) is presented in Fig. 15.

4. Discussion

4.1. Glass transition

Table 1 shows that the value of T_g increases with the heating rate (β), and it was verified that the dependence of T_g on β was expressed according to Lasocka equation [16]. The activation energy for glass transition (E_g), which is associated with the molecular motion and rearrangement of atoms around T_g , was calculated by the Kissinger equation [15], and its simplified form [17], giving values that are in close agreement ($537 \pm 16 \text{ kJ mol}^{-1}$ and $550 \pm 16 \text{ kJ mol}^{-1}$, respectively). These values are higher than those obtained for a terbium-doped lithium aluminophosphate glass, 462 and 475 kJ mol^{-1} [8].

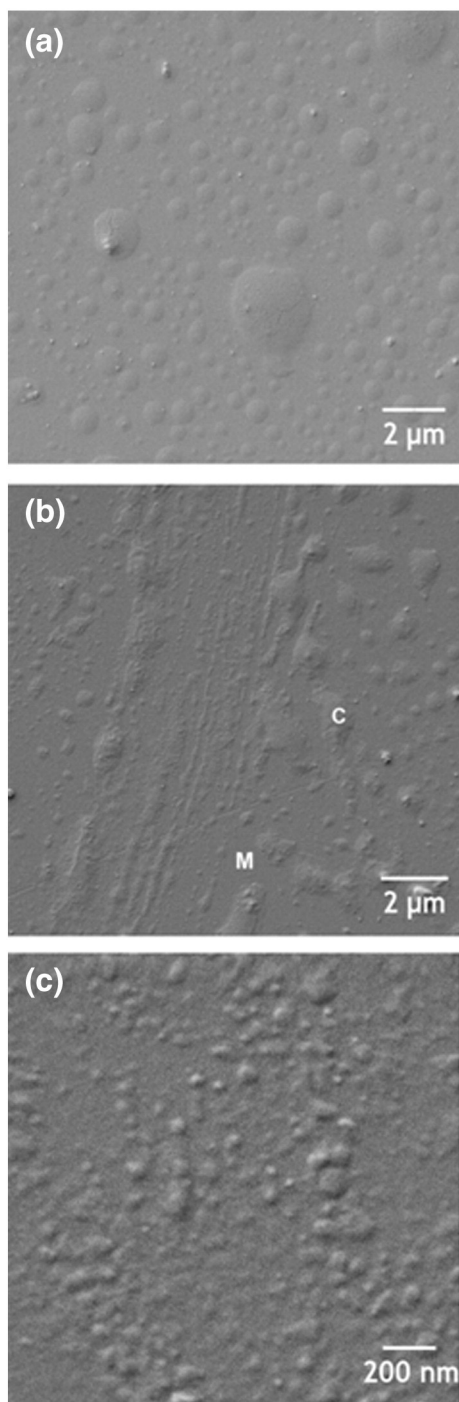


Fig. 14. SEM of glass samples heat-treated for 2 h at 823 K (a) and at 923 K (b and c).

4.2. Crystallization kinetics

All the DTA curves (Fig. 1) show two broad exothermic peaks associated with the appearance of crystalline phases. From Table 1 it is observed that the onset (T_{c1} and T_{c2}) and peak crystallization temperatures (T_{p1} and T_{p2}) increase with β . The thermal stability of the glass, corresponding to the temperature difference between T_{c1} and T_g , increases from 34 to 57 K with the increase in β from 5 to 25 K min⁻¹.

By monitoring the shift in the position of the exothermic peaks as a function of β , the kinetic parameters (crystallization activation energy (E_c) and Avrami exponent (n), related to the glass crystallization process) were evaluated. From Table 2 it is observed that the values of E_{c1} and E_{c2} calculated according Kissinger method (398 ± 14 and $162 \pm$

14 kJ mol⁻¹, respectively) were in close agreement with those obtained by the Ozawa method (412 ± 14 and 179 ± 14 kJ mol⁻¹, respectively).

To study the nature of the crystallization process, the fraction of crystallization (χ) as a function of temperature was determined for both exothermic peaks, and the graphical representation (Fig. 6) shows typical sigmoid curves for the different heating rates, indicating that the formation of crystalline phase proceeded by a combination of nucleation and growth processes [27]. From Fig. 7, it is observed that the maximum crystallization rate, $(d\chi/dt)_{Tp}$, increases with the increase in β , as it has been reported in the literature [21]. The Avrami exponent was calculated by the Gao–Wang model [20–22], which has been developed assuming that nucleation is randomly distributed and the growth rate of the new phase depends mainly on the temperature rather than duration of the heating time [22]. Allowing for the experimental error, the value of $\langle n \rangle$ is close to 1 for both peaks (see Table 2). Comparing the value estimated for the Avrami exponent with the theoretical values [28], it is suggested that surface crystallization ($n \approx 1$) is dominant during the crystallization of the glass associated with the first and second peaks.

An isoconversional method was employed to determine the activation energy of crystallization as a function of χ . From Fig. 10(a) it is noticed that, for the first exothermic peak, the average value of $E_{c1}(\chi)$ is in the range of 380–400 kJ mol⁻¹, being comparable to the values of E_{c1} listed in Table 2, obtained by different methods. For the second exothermic peak, the average value of $E_{c2}(\chi)$ is in the range of 125–150 kJ mol⁻¹ ($\chi = 0.2$), and it decreases continuously to 90–105 kJ mol⁻¹ ($\chi = 0.8$), as shown in Fig. 10(b). These results suggest that, during the heating in the temperature range within the second exotherm, with the progression of the crystallized fraction less activation energy is necessary for the occurrence of further crystallization. It is observed that, for the various heating rates, the average value of $n(\chi)$ is about 0.8 for the first peak, Fig. 11(a), and that the average value of $n(\chi)$ for the second peak varies from 1.3 to 2 with the increase in χ , Fig. 11(b). Comparing the values calculated for $n(\chi)$ with the theoretical values [28], a surface crystallization mechanism may be considered for the crystallization process associated with the first and second exothermic peaks at the various heating rates.

Few works have been reported in the literature regarding the crystallization kinetics of RE-doped lithium aluminophosphate glasses. The compositions of the studied glasses and the sample particle sizes were different, which may have a serious impact on the crystallization process. Fang et al. [7] studied the crystallization kinetics of a glass with a slightly different composition, co-doped with $0.5\text{Er}^{3+}/2\text{Yb}^{3+}$ ($<210 \mu\text{m}$) and obtained a value of $E_c \approx 190$ kJ mol⁻¹, but did not report a value for n . Soares et al. [8] investigated the crystallization kinetics of a Tb^{3+} -doped glass ($<65 \mu\text{m}$) and found $E_c \approx 270$ kJ mol⁻¹ and $n \approx 1$.

4.3. Phase assemblage and microstructure

The XRD results (Fig. 12) revealed that the glass sample heat-treated at 773 K was still amorphous, and that by heating the glass samples to temperatures higher than T_{c1} they undergo a complex crystallization process leading to the formation of different crystalline phases. In glass samples treated at 823 and 923 K, the predominant phase was cubic aluminum metaphosphate, $\text{Al}(\text{PO}_3)_3$, but the intensity of the peaks slightly decreased with an increasing heat treatment (Fig. 12c–d). Aluminum phosphate, AlPO_4 , in the rhombohedral form appeared in samples treated at both temperatures, and peaks of orthorhombic form were also identified at the highest temperature. The presence of lithium barium phosphate, $\text{Li}_3\text{Ba}_2(\text{PO}_3)_7$, was identified in the glass sample treated at 823 K, but it was not detected in the glass sample treated at 923 K, where barium pyrophosphate, $\text{Ba}_2\text{P}_2\text{O}_7$, was identified. It has been verified that the crystallization of aluminophosphate based glasses containing different compounds (e.g., Li_2O , Na_2O) yields frequently aluminum metaphosphate and aluminum phosphate, which is present as a secondary phase [8,29]. Langlet et al. [29] reported

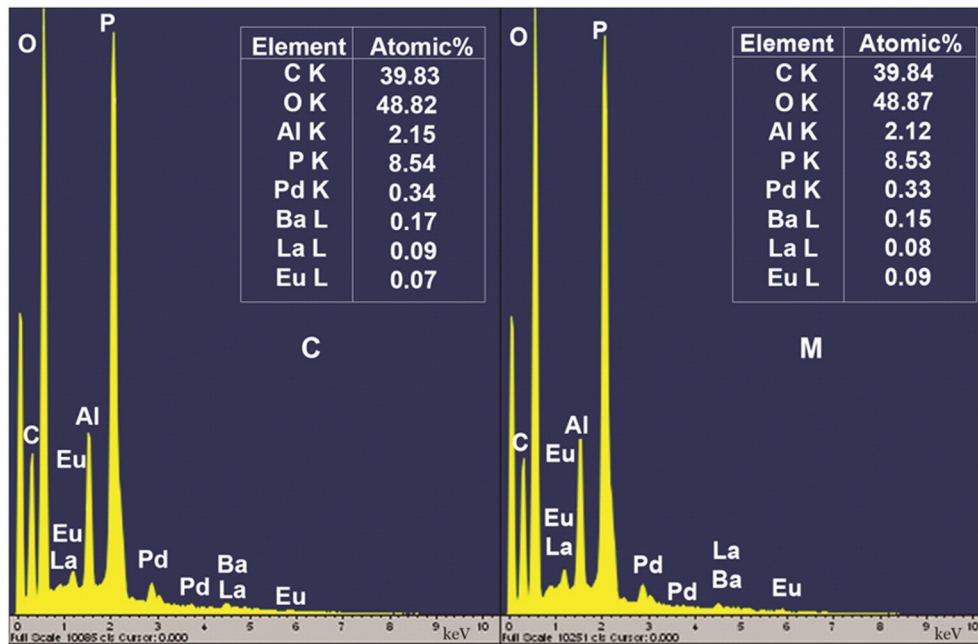


Fig. 15. EDS spectrum of glass sample heat-treated at 923 K.

that cubic aluminum metaphosphate is the only form stable at high temperature among the five known $\text{Al}(\text{PO}_3)_3$ species, and they identified the formation of two forms of AlPO_4 , resulting from P_2O_5 loss during the melting process and that was formed at the surface of the glass samples.

Evidence of surface crystallization was noticeable in the glass sample treated for 2 h at 823 K, as shown in the optical microscopy image under cross-polarized light, Fig. 13(a), where “flower-like” aggregates of crystals radially grown in a non-uniform glass matrix are observed. After 2 h treatment at 923 K well developed “flower-like” aggregates, having an average size of $\sim 100 \mu\text{m}$, were observed inside the glass matrix, but in smaller number. SEM analysis revealed the presence of round-shape precipitates, with an average size smaller than $1 \mu\text{m}$, in the glass matrix of the sample heated at 823 K, Fig. 14(a). With further heating, the shape of the precipitates was altered, Fig. 14(b), and at higher magnification, Fig. 14(c), nano-crystallites dispersed all over the glass matrix were observed. The elemental chemical analysis by EDS of the precipitates has not been conclusive due to their small size compared to the detection width of the microanalysis probe ($\sim 1 \mu\text{m}$ size), and similar results were obtained for the precipitates (C) and matrix (M) regions identified in Fig. 14(b). The spectra obtained by EDS elemental analysis (Fig. 15) reveal peaks of identical intensity, corresponding to the elements that are present in the glass composition with the exception of Li, that is very light for detection. Identification of Pd and C was due to sample preparation.

The results presented in this work indicated that no phase formation occurred when the glass was heat-treated at 773 K and that different phosphate phases appeared with increasing temperature. A future extension of the present study will be the investigation of the relationship between structural changes and the optical absorption and luminescence properties of the crystallized glasses.

5. Conclusions

The thermal transformation and crystallization kinetics of a Eu^{3+} doped lithium aluminophosphate glass composition have been studied by DTA, XRD, and SEM. DTA curves exhibited an endothermic peak and two exothermic crystallization peaks. The thermal stability of the glass increased with the heating rate. No phase formation was detected in the glass when heated up to 773 K. The glass was found to crystallize

into a mixture of $\text{Al}(\text{PO}_3)_3$ and AlPO_4 with $\text{Li}_3\text{Ba}_2(\text{PO}_3)_7$ during the first exothermic peak, and a mixture of $\text{Al}(\text{PO}_3)_3$ and AlPO_4 with $\text{Ba}_2\text{P}_2\text{O}_7$ during the second crystallization peak. The activation energy of crystallization for the first exothermic peak was higher than for the second peak. The estimated values of the Avrami exponent suggest that the process involved in the crystallization of the glass is surface crystallization for both exothermic peaks. Surface crystallization was also suggested from microstructural analysis.

Acknowledgments

The authors are grateful to the FCT (Foundation for Science and Technology), Portugal, for financing ERA-MNT/001/2010, PTDC/CTM/102141/2008 and PEst-C/CTM/LA0025/2013, projects, and to the UEFISCDI (Executive Unity for Financing of Higher Education, Research and Innovation), Romania, for the financial support in the frame of 7-031/2011 MNT-ERA.NET contract and 168/2012 Project from Partnership Programme.

References

- [1] A. Schülzgen, L. Li, D. Nguyen, Ch. Spiegelberg, R. Matei Rogoian, A. Laronche, J. Albert, N. Peyghambarian, Distributed feedback fiber laser pumped by multimode laser diodes, *Optics Lett.* 33 (2008) 614–616.
- [2] C. Nico, R. Fernandes, M.P.F. Graça, M. Elisa, B.A. Sava, R.C.C. Monteiro, L. Rino, T. Monteiro, Eu^{3+} luminescence in aluminophosphate glasses, *J. Lumin.* 145 (2014) 582–587.
- [3] N.V. Nikonov, G.T. Petrovskii, Ion-exchanged glasses in integrated optics: the current state of research and prospects (a review), *Glass Phys. Chem.* 25 (1999) 16–55.
- [4] M. Elisa, B.A. Sava, I.C. Vasiliu, R.C.C. Monteiro, J.P. Veiga, L. Ghervase, I. Feraru, R. Iordanescu, Optical and structural characterization of samarium and europium-doped phosphate glasses, *J. Non-Cryst. Solids* 369 (2013) 55–60.
- [5] C. Nico, M.P.F. Graça, M. Elisa, B.A. Sava, R.C.C. Monteiro, L. Rino, T. Monteiro, Effects of ultraviolet excitation on the spectroscopic properties of Sm^{3+} and Tb^{3+} doped aluminophosphate glasses, *Opt. Mater.* 35 (2013) 2382–2388.
- [6] C. Shen, S. Baccaro, Z. Xing, Q. Yan, S. Wang, G. Chen, Different luminescence behaviors of $\text{SnO}_2/\text{Eu}^{3+}$ and $\text{SnO}_2/\text{Tm}^{3+}$ co-doped phosphate glasses, *Chem. Phys. Lett.* 492 (2010) 123–126.
- [7] Y. Fang, M. Liao, L. Hua, Effect of lithium–sodium mixed-alkali on phase transformation kinetics in $\text{Er}^{3+}/\text{Yb}^{3+}$ co-doped aluminophosphate glasses, *Thermochim. Acta* 443 (2006) 179–182.
- [8] R.S. Soares, R.C.C. Monteiro, M.M.R.A. Lima, B.A. Sava, M. Elisa, Phase transformation and microstructural evolution after heat treatment of a terbium-doped lithium phosphate glass, *J. Mater. Sci.* 49 (2014) 4601–4611.
- [9] W.A. Johnson, R.F. Mehl, Reaction kinetics in processes of nucleation and growth, *Trans. AIME* 135 (1939) 416–442.

- [10] M. Avrami, Kinetics of phase change. I General theory, *J. Chem. Phys.* 7 (1939) 1103–1112.
- [11] M. Avrami, Transformation–time relations for random distribution of nuclei, *J. Chem. Phys.* 8 (1940) 212–224.
- [12] M. Avrami, Kinetics of phase change. III Granulation, phase change, and microstructure, *J. Chem. Phys.* 9 (1941) 177–184.
- [13] B.A. Sava, M. Elisa, L. Boroica, R.C.C. Monteiro, Preparation method and thermal properties of samarium and europium-doped aluminophosphate glasses, *Mater. Sci. Eng. B* 178 (2013) 1429–1435.
- [14] M. Lasocka, The effect of scanning rate on glass transition temperature of splat-cooled $\text{Te}_{85}\text{Ge}_{15}$, The second international conference on rapidly quenched metals, *Mater. Sci. Engineering*, 23, 1976, pp. 173–177.
- [15] H.E. Kissinger, Reaction kinetics in differential thermal analysis, *Anal. Chem.* 29 (1957) 1702–1706.
- [16] N. Tanwar, V.K. Saraswat, A study of kinetics of phase transformation of $\text{Ge}_{10}\text{Se}_{75}\text{Sb}_{15}$ chalcogenide glass, *J. Non-Cryst. Solids* 394–395 (2014) 1–5.
- [17] S. Mahadevan, A. Giridhar, A.K. Singh, Calorimetric measurements on As–Sb–Se glasses, *J. Non-Cryst. Solids* 88 (1986) 11–34.
- [18] T. Ozawa, Kinetics of non-isothermal crystallization, *Polymer* 12 (1971) 150–158.
- [19] A. Arora, E.R. Shaaban, K. Singh, O.P. Pandey, Non-isothermal crystallization kinetics of ZnO–BaO– B_2O_3 – SiO_2 glass, *J. Non-Cryst. Solids* 354 (2008) 3944–3951.
- [20] Y.Q. Gao, W. Wang, On the activation energy of crystallization in metallic glasses, *J. Non-Cryst. Solids* 81 (1986) 129–134.
- [21] J. Vázquez, C. Wagner, P. Villares, R. Jiménez-Garay, Glass transition and crystallization kinetics in $\text{Sb}_{0.18}\text{As}_{0.34}\text{Se}_{0.48}$ glassy alloy by using non-isothermal techniques, *J. Non-Cryst. Solids* 235–237 (1998) 548–553.
- [22] B. Shanmugavelu, V.V.R.K. Kumar, Crystallization kinetics and phase transformation of bismuth zinc borate glass, *J. Am. Ceram. Soc.* 95 (2012) 2891–2898.
- [23] K. Matusita, T. Komatsu, R. Yokota, Kinetics of non-isothermal crystallization process and activation energy for crystal growth in amorphous materials, *J. Mater. Sci.* 19 (1983) 291–296.
- [24] W. Lu, B. Yan, W. Huang, Complex primary crystallization kinetics of amorphous Finemet alloy, *J. Non-Cryst. Solids* 351 (2005) 3320–3324.
- [25] H.L. Friedman, Kinetics of thermal degradation of char-forming plastics from thermogravimetry. Application to a phenolic plastic, *J. Polym. Sci. C Polym. Symp.* 6 (1965) 183–195.
- [26] T. Ozawa, Applicability of Friedman plot, *J. Therm. Anal.* 31 (1986) 547–551.
- [27] J.-H. Jean, Y.-C. Fang, S.X. Dai, D.L. Wilcox, Devitrification kinetics and mechanism of K_2O –CaO–SrO–BaO– B_2O_3 – SiO_2 glass–ceramic, *J. Am. Ceram. Soc.* 84 (2001) 1354–1360.
- [28] S.H. Park, H.C. Lee, B.K. Ryu, M.M. Son, H.S. Lee, I. Yasui, Nucleation and crystallization kinetics of CaO– Al_2O_3 – 2SiO_2 in powdered anorthite glass, *J. Mater. Sci.* 31 (1996) 4249–4253.
- [29] M. Langlet, M. Saltzberg, R.D. Shannon, Aluminium metaphosphate glass–ceramics, *J. Mater. Sci.* 27 (1992) 972–982.